A Study of Geometry and Roughness Effects to Nanoindentation Hardness Tests

*Roger Y. Lo, David B. Bogy, and C. Singh Bhatia**

Computer Mechanics Laboratory
Department of Mechanical Engineering
University of California, Berkeley
Berkeley, CA 94720

** Storage Systems Division, IBM Corporation*
5600 Cottle Road
San Jose, CA 95193

ABSTRACT

The assumption of flat and smooth specimen surfaces is not valid when the indentation sizes are forced to be comparable to that of the surface roughness. The existence of surface curvature and roughness brings errors and variations to the nanoindentation measurements of thin film mechanical properties. A model based on the Hertz contact theory is modified and used to study the influence of specimen surface curvature on nanoindentation measurements. This model is then adopted to study the measurement variations due to surface roughness. Random location indentations are then performed on these surfaces with three different loads. The concept of apparent surface properties to the indenter has been proposed. The roughness effect is defined as the standard deviation of the measurements to the their mean values. The results show that this model predicts the roughness effect very well for very shallow indentations with only the knowledge of the surface roughness.

1. INTRODUCTION

Nanoindentation techniques together with the theoretical analyses in Lo and Bogy (1997) and Lo and Bogy (1999) are used to evaluate the mechanical properties of thin films materials. The theoretical analyses in these papers assume that the surface of the specimen is mathematically smooth and flat. However, real surfaces always have surface curvature and roughness. Calculations based on these models give accurate results when the specimen surface is atomically smooth (e.g. Silicon wafer), or the indentations are much larger or smaller than the size of the surface roughness. When the indentation depths are much larger than the heights of roughness, the indenter contacts with many asperities while pushing into the surface. The contact areas at maximum depths are much larger than the diameters of single asperities. In this case, the existence of surface roughness only creates a minor variation of the measurements. In fact, Tabor (1951) noted that the surface roughness could be taken into consideration by adding a constant term to the displacement of the indenter. When the indentation depths are much smaller than the heights of the roughness, the indenter may only contact with one single asperity on the surface. If the asperity is much larger than the indentation in height and diameter, the flat and smooth surface assumptions are still applied. Questions arise if the indentation size is comparable to that of the surface roughness. In preparation for the expected the future areal density on magnetic disks, thin film overcoats with thickness of 2 nm to 5 nm are already under development. The typical size of the roughness of these films is around 0.6 nm in R_a (which will be defined later). To avoid the substrate effect on the measurements, residual indentation depths have to be smaller than 0.4

nm to 1 nm. Therefore, indentation sizes similar to that of the surface roughness seem to be inevitable.

The study of contacts between rough surfaces can be traced back to Greenwood and Williamson (1966). They considered the contact of a flat two-dimensional plane with a nominally flat rough surface. They assumed spherical asperities and a Gaussian distribution of asperity heights. They were able to obtain the real total contact area and total contact force by applying the Hertz contact theory on every asperity. Greenwood and Tripp (1967) adopted similar concept to study the contacts between rough curved surfaces. Their methods are good for large indenters contacting with relatively small asperities. More insight is needed to study single asperity contacts. Bobji et al (1996) studied single asperity contact with offset from the centerline of the indenter by a simple geometry analysis. They obtained the following relation,

$$\frac{H_{measured}}{H_{true}} = \left(\frac{R}{R_0} \right) \cos^2 \theta \, . \tag{1}$$

The measured surface hardness is related to the true hardness through the geometry factors, which will be defined later. However, their derivation is lacking in terms of mechanics. In this paper, the above relation is re-derived using Hertz contact theory, and it is shown that the quantity in the parenthesis should have a power of 2/3, instead of one. Experimental verification is also provided.

Next, the single asperity contact model is used to study the variation of hardness measurements on rough surfaces. The goal is to relate the variation of hardness measurements to the standard deviation of the roughness properties, such as the quantity in

the parenthesis in Eq. (1). The concepts of apparent roughness and apparent radius of curvature of the specimen to the indenter are proposed. Experimental results show that the hardness variation increases as the indentation sizes decreases and thus, gets close to the surface roughness dimension. At extremely shallow indentations, the ratio of standard deviation of the hardness measurements over the mean hardness on one surface equals the apparent standard deviation of $\left(\frac{R}{R_0}\right)^{\frac{2}{3}}$ for that surface. In addition, it is shown that a blunter indenter experiences less “roughness effect”.

2 THEORETICAL DEVELOPMENT

2.1 Indentations on bumps of solids of revolution

Here we first review the results presented in Lo and Bogy (1999). When two solids are brought into contact, they initially touch at a single point or along a line. As the contact force increases, they deform near their points of first contact. With help from the Hertz contact theory, we are able to show that the separation s between the surfaces of two solids of revolution contacting at their apex points is,

$$s = \frac{r^2}{2R}. \tag{2}$$

$$\text{where, } \frac{1}{R} = \frac{1}{R_1} + \frac{1}{R_2} \tag{3}$$

R is the relative radius of the system at the point of the contact; R_1 and R_2 are the radii of curvature of body 1 and body 2 at the points of contact; $r = \sqrt{x^2 + y^2}$ is radial coordinate. Figure 1 shows the geometry of two solids of revolution in contact under the application of a normal load P. Body 1 is taken as the indenter and body 2 is the specimen. u_{z1} and u_{z2} are the displacements of points S_1 on the indenter and S_2 on the specimen due to the contact pressure. h_1 and h_2 are the displacements of distant points in the two bodies T_1 and T_2. a is the radius of the contact circle. After deformation, if the points S_1 and S_2 coincide with each other within the contact surface, then

$$u_{z1} + u_{z2} + s = h_1 + h_2 = h\,, \tag{4}$$

where h is the relative displacement of two distant points T_1 and T_2. Equation (4) has to be satisfied for all points within the contact circle, i.e. for $0 \le r \le a$, where a is the contact radius, i.e. the radius of the contact circle. Substituting Eq. (2) into Eq. (4), we obtain,

$$u_{z1} + u_{z2} = h - \frac{r^2}{2R}. \tag{5}$$

The pressure distribution obtained by Hertz, which results in displacements satisfying Eq. (5), is given by

$$p = p_0 \left[1 - \left(\frac{r}{a} \right)^2 \right]^{1/2}, \; r \le a, \tag{6}$$

where p_0 is the maximum pressure. The displacement for both solids can be written as,

$$u_{zi} = \frac{1 - \nu_i^{\,2}}{E_i} \frac{\pi p_0}{4a} \left(2a^2 - r^2 \right), \; r \le a. \tag{7}$$

where i = 1, 2. Therefore, Eq. (7) can be written as,

$$h = \frac{\pi p_0}{4aE_r} \left(2a^2 - r^2 \right) + \frac{r^2}{2R}, \tag{8}$$

where $\frac{1}{E_r} = \frac{1-\nu_1^2}{E_1} + \frac{1-\nu_2^2}{E_2}$, E_r the reduced modulus of the system, and h and a are variables independent of r. Since the left hand side is not a function of r, the right hand side cannot be a function of r. Therefore, the coefficient of r^2 must vanish, and we have

$$\frac{\pi p_o}{4aE_r} = \frac{1}{2R}, \tag{9}$$

or,

$$a = \frac{\pi p_0 R}{2E_r}. \tag{10}$$

Substituting Eq. (10) back into Eq. (8), we obtain

$$h = \frac{\pi a p_0}{2E_r} = \frac{a^2}{R}. \tag{11}$$

The total load can also be calculated by integrating the pressure over the contact area, i.e., $P = \int p(r) 2\pi r dr = 2/3 p_0 \pi a^2$. Substituting for p_0 by $\frac{3}{2}\frac{P}{\pi a^2}$ into Eq. (10) and Eq. (11), we have,

$$a = \left(\frac{3PR}{4E_r}\right)^{1/3}, \tag{12}$$

$$h = \frac{a^2}{R} = \left(\frac{9P^2}{16RE_r^2}\right)^{1/3}. \tag{13}$$

The second equality in Eq. (13) can be re-written as,

$$P = \frac{4}{3} E_r \sqrt{Rh^3}. \tag{14}$$

Taking the first derivative of P with respect to h, we obtain

$$\frac{dP}{dh} = 2E_r \sqrt{Rh} = 2aE_r = 2\sqrt{\frac{A}{\pi}} E_r, \tag{15}$$

in which the first equality of Eq. (13) and $A = \pi a^2$ have been invoked.

The restrictions of this derivation are that the contact radius has to be much smaller than the tip radius as well as the lateral and axial dimensions of the two bodies. That is to say $a << R$, and $a << l$, where l represents the lateral and axial dimensions of the bodies. These restrictions simply mean that the tip radius R can be taken as a constant if the contact radius a is relatively small. Therefore, the indenter can be viewed as a spherical body in the contact area if the contact area is small enough.

2.2 Indentations on a bump of solid of revolution with offsets

The theoretical development in the previous section is valid for solids of revolution contacting at their apex points. In this section, contacts of slightly offset solids of revolutions are studied. At the same time, comparison between the measured and true hardnesses in the presence of surface curvature is also discussed.

Figure 2 shows a schematic diagram for contacts between two solids of revolution with an offset angle θ, which is assumed to be very small so that both of the radii of curvature for the two solids in the contact region are constant. This means that the deformations on both solids are localized in their spherical regions. The load applied by the indenter is P and the vertical displacement is h. However, the normal load and normal displacement relative to the specimen are P_n and h_n, respectively. Assuming no friction between the two solids, the method presented in the previous section is able to model the contact between them with P_n (= $P \cos\theta$) and h_n (=$h \cos\theta$) substituting P and h in Eqs. (12) to (15), respectively. Sliding between the solids while the indenter is moving into the surface may violate the condition modeled in the previous section. However, the restriction of very small θ prevents the sliding effect from becoming a major issue. According to the first equality of Eq. (13), the contact area is directly proportional to the contact depth. Thus, the normal contact area can be written as

$$A_n = \pi h_n R = (\pi h R)\cos\theta = A\cos\theta \tag{16}$$

where A is the contact area without offset and R is the relative radius of curvature of the system.

From Eq. (3), the value of R achieves its maximum when R_2 approaches infinity (i.e. a flat specimen surface). We denote the maximum value of R as R_0, which equals the indenter tip radius R_1. The values obtained from Eqs. (13), (14), and (15) with R_0 are denoted with a subscript *0*, i.e. a_0, h_0 and S_0, and are written below

$$a_0 = \left(\frac{3R_0 P}{8E_r} \right)^{1/3}, \tag{17}$$

$$h_0 = \left(\frac{9P}{8R_0 E_r} \right)^{1/3}, \tag{18}$$

$$S_0 = \frac{dP}{dh_0} = 2a_0 E_r . \tag{19}$$

In addition, the contact area for indentation on a flat surface can be written as

$$A_0 = \pi a_0^2 . \tag{20}$$

The ratio of the contact area with specimen surface curvature A to the contact area for a flat surface is obtained with Eqs. (12), (17), (20), and the relation, $A = \pi a^2$,

$$\frac{A}{A_0} = \left(\frac{R}{R_0} \right)^{\frac{2}{3}} . \tag{21}$$

Since the Hysitron Picoindenter only measures the vertical load, P and vertical displacement, h, the machine does not take into account the surface curvatures and possible offsets. The contact area calculated from the method provided in Lo and Bogy (1999) with the measured P and h is the equivalent contact area for a flat surface, rather than the real contact area. Therefore, the calculated hardness based this area is not the true hardness of the

specimen. By using Eqs. (16), (21), and the definition of hardness, we derive the measured hardness as follows,

$$H_{measured} = \frac{P}{A_0} = \frac{P_n cos\theta}{A}\left(\frac{R}{R_0}\right)^{\frac{2}{3}} = \frac{P_n}{A_n}\left(\frac{R}{R_0}\right)^{\frac{2}{3}} cos^2\theta$$

where P_n / A_n is the true hardness of the specimen. Thus, we have,

$$\frac{H_{measured}}{H_{true}} = \left(\frac{R}{R_0}\right)^{\frac{2}{3}} \cos^2\theta \qquad (22)$$

Eq. (22) is very similar to Eq. (1), which is obtained by Bobji *et al* (1996) except that they derived a power of one for the quantity in the parenthesis. The experimental verification for Eq. (22) will be provided in the next section. If the surface of the specimen is flat, Eq. (22) gives $H_{measured} = H_{true}$, since $R = R_0$ and $\theta = 0$. Thus, the true hardness can be obtained on a flat surface and is also called the flat hardness. If the indentation tests are done on a convex part of the surface such as a bump or an asperity ($R < R_0$), the measured hardness is always smaller than the true hardness. It is not difficult to visualize this result with the help of Figure 3.The load and displacement recorded by the Hysitron Picoindenter is the vertical load *P* and the vertical displacement *h*. With the assumption of a flat surface, the analysis roughly distributes the resistance from the material over the entire region under the horizontal line, including the excess region. However, the resistance only comes from the bump region. Therefore, the analysis based on a flat surface underestimates the resistance thus, the hardness of the specimen. It is worth noting that if the bump radius is much larger than the indenter tip radius ($R \approx R_0$), the measured hardness based on the flat surface assumption is a good approximation to the true hardness.

The offset between the indenter and the specimen lowers the measured hardness by the amount of $\cos^2\theta$. Since the model requires θ to be small, the offset influence $\cos^2\theta$ is also small. For example, $\cos^2\theta$ lowers the measured hardness by about 10% if θ equals 20 degrees.

3 EXPERIMENTS

In order to verify Eq. (22), nanoindentation tests are first carried out on the top of "Sombrero" type laser bumps of 5 μm to 10 μm in diameter and 20 nm to 30 nm in height. The laser bumps are of the type often used in the parking zones on hard disks to avoid stiction between the sliders and disks. Assuming the bump tips are spherical, their radii of curvature are estimated between 100 μm and 600 μm. These radii are 3 to 4 orders larger than the tip radii, which range from 50 nm to 200 nm. The term in the parenthesis in Eq. (22) therefore has the value close to one for all the bumps. So there is essentially no difference between $H_{measured}$ and H_{true}. To have an effect from the surface curvature, bump radii close to the tip radii are needed.

3.1 Nanoindentations on asperities

Since it is difficult to find machined surfaces with bump radii of curvature of 50 nm to 200 nm, nanoindentation tests were performed on the asperities of regular hard disk surfaces. Asperities with shapes close to spherical were chosen to be the targets. The indenter was carefully moved to the top of the asperities so that θ in Eq. (22) is zero. Before each test, the area around the targeted asperity was scanned with the Hysitron Picoindenter. The radius of curvature of the asperity was then calculated by assuming the asperities are spherical. The ratio of (R/R_0) were then calculated for each asperity with this radius and the known tip radius. Indentation forces have to be small enough to avoid plastic deformation and

interaction with the non-spherical bases of the asperities. In other words, the indentation forces were chosen to elastically deform the very top portion of the asperities. Based on this requirement, the indentation forces ranged from 20 μN to 50 μN depending on the specimen hardnesses and the indenter tip radii.

Figure 4 shows the ratio of the measured hardness to the true hardness vs. R/R_0. The functions, $\frac{H_{measured}}{H_{true}} = \left(\frac{R}{R_0}\right)^{\frac{2}{3}}$ and $\frac{H_{measured}}{H_{true}} = \left(\frac{R}{R_0}\right)$, are also plotted. The smallest asperity radius found was 250 nm while most radii were about 500 nm. Since the indenter tip radius was 186 nm, all of the data points in Fig. 4 fall in upper portion of the curve. The function of power of 2/3 fits the data shown very well. When R/R_0 equals 0.57, the measured hardness is about 70 % of the true specimen hardness. The difference between the function of power of 2/3 and the linear one is about 15% at R/R_0 of 0.6 and 0 when R/R_0 equals 1. Asperities with radius smaller than 250 nm are rare on disk surfaces. It is even more difficult to indent these asperities without plastic deformation or interaction with their non-spherical bases. Thus, the lower portion of the curve in Fig. 4 is left empty.

3.2 Random indentations

The model has been verified by indentations on single asperities in the previous section. Questions arise as to how well this model predicts measurement variations on rough surfaces. Therefore, indentations on rough surfaces were performed randomly to study the

measurement variations. The indenter was moved laterally 1 μm for a sequence of indentations with the scan size staying at zero. In other words, each indentation was made without the knowledge of the local surface topography around the indentation location. Thus, indentations were made on asperities as well as in the concave areas on the surface. The hardness value for each indentation was then calculated with the obtained load/displacement curves. The mean values, $\overline{H}$, and standard deviations, S_H, for all the tests were then calculated. The standard deviation of a set of data x is defined as,

$$S_x^2 = \frac{1}{n}\sum_{i=1}^{n}\left(x_i - \bar{x}\right)^2 \tag{23}$$

where n is the number of data obtained. Two samples were tested with two indenters of different tip radii. The samples were 100 nm hydrogenated carbon (CH_x) and nitrogenated (CN_x) films. The standard deviation of the surface roughness and R_a of sample A were 0.822 nm and 0.63 nm, respectively. The standard deviation of the surface roughness and R_a of sample B were 0.697 nm and 0.548 nm, respectively. R_a is defined as

$$R_a = \frac{1}{A}\iint_A |z(x)|dx\,. \tag{24}$$

where $z(x)$ is the roughness height function relative to the mean height of the surface. Both indenters were cube-corner diamonds with tip radius of 186 nm for Tip 1 and 56 nm for Tip 2. Figure 5 shows the hardness values for 50 random indentations on sample A indented by Tip 2. The mean hardness and standard deviation are 16.126 GPa and 3.527 GPa, respectively. The mean hardness is taken as the flat or true hardness in Eq. (22), which

implies that the ratio $\frac{H_{measured}}{H_{flat}}$ equals to $\left(\frac{R}{R_0}\right)^{\frac{2}{3}}$ when θ is zero. We assume that θ is small enough that $\cos^2\theta$ in Eq. (22) can be ignored. Next we wish to study how well the standard deviation of the variation of $\frac{H_{measured}}{H_{flat}}$ agrees with the standard deviation of the variation of $\left(\frac{R}{R_0}\right)^{\frac{2}{3}}$. Since the mean hardness $\overline{H}$ (or H_{flat}) is a constant, the standard deviation of $\frac{H_{measured}}{H_{flat}}$ can be expressed as

$$S_{\frac{H_m}{\overline{H}}} = \frac{S_{H_m}}{\overline{H}} \tag{25}$$

Therefore, we just need to compare the ratio of standard deviation of hardness variation S_{H_m} to the mean hardness $\overline{H}$ with the standard deviation of $\left(\frac{R}{R_0}\right)^{\frac{2}{3}}$. The ratio in Eq. (25) is called the roughness effect on nanoindentation hardness measurements. Table 1 lists the measured hardness values, the mean hardness values, and their ratios for both samples indented by both indenters. Three random indentations with various indentation forces were performed on each sample. The maximum depths ranged from 4 nm to 16 nm. Since the maximum differences in asperity heights of both samples are within 5 nm, it is expected that the contact model loses its accuracy for indentations of maximum depths larger than or comparable to 5 nm.

Next, we turn our focus to finding the standard deviation of $\left(\frac{R}{R_0}\right)^{\frac{2}{3}}$ for both surfaces.

Since not all of the asperities and the concave areas on the surface are spherical or close to spherical, special care is needed to implement the contact model. Greenwood (1967) and Ling (1973) indicated that it is sufficient to characterize a random surface with a profilometric representation along a straight line. Therefore, a line with the same roughness standard deviation as the entire surface is chosen to represent each of the two disk surfaces with the assumption that the surfaces are random. Figure 6 shows a typical scanned line of sample A. Note that the vertical dimension has been exaggerated. The asperities on this line are then approximated by solids of revolution with spherical top portions. If z_{i+1}, z_i, and z_{i-1} are three consecutive heights on the scanned line, according to Johnson (1987), the curvature is defined by,

$$\kappa_i = \frac{z_{i+1} - 2z_i + z_{i-1}}{h^2}, \tag{26}$$

where h is the length of the increment intervals in nanometers and κ_i is the curvature of the ith data point. For an image of 1 μm by 1 μm scanned with 256 lines, h equals 3.90625 nm. The radius of curvature is obtained by taking the reciprocal of κ_i, i.e. $r_i = 1/\kappa_i$. With the assumption of asperities of solids of revolution, the radii of curvature of one asperity in both principal directions are r_i. A positive r_i represents an asperity; while a negative one indicates a cavity on the surface. All asperities with positive radii are likely to be hit by the indenter during random indentations. However, the indenter is not able to reach the cavities whose radii are smaller than the indenter tip radius. For simplicity, we disregard these

cavities. This means that we view these areas as flat. Therefore, the statistical properties of the surface such as the standard deviation of roughness will be slightly changed due to this simplification. The modified radii of curvature are called the apparent radii of curvature for the indenters. Since different indenters have different tip radii, the apparent radii of curvature of the surface are different for the indenters. It is expected that the standard deviation of the apparent radii of curvature of the same surface is larger for sharper indenters. Recall that the effective radius of curvature R_i of the indenter/specimen system is defined as,

$$\frac{1}{R_i} = \frac{1}{r_i} + \frac{1}{R_0}. \tag{27}$$

Table 2 lists the standard deviation of the apparent radii of curvature as well as other statistical properties for both sample surfaces for both indenters. It is not a surprise that Sample A has smaller mean radii of curvature and standard deviation of radii of curvature than Sample B, since Sample A is rougher. The standard deviation of $\left(\frac{R_i}{R_0}\right)^{\frac{2}{3}}$ for Sample A is larger than that of Sample B due to the same reason. Cross-comparison of the surface properties for different indenters suggests that surface roughness has stronger influence for a sharper indenter. This finding also agrees with our intuition.

The standard deviations of $\left(\frac{R_i}{R_0}\right)^{\frac{2}{3}}$ are compared with the hardness measurements obtained earlier. Figures 7 and 8 show the ratios of the standard deviation to mean hardnesses for Sample A and Sample B, respectively. Each data point in the figures represent the result

from 50 random indentation tests. The standard deviation of $\left(\frac{R_i}{R_0}\right)^{\frac{2}{3}}$ for each combination is listed in the legend. From both figures, it is seen that the standard deviation to mean ratio increases as the maximum decreases. This implies that the deformation mechanism for smaller indentation depths is closer to the assumptions of the contact model, because the indentation sizes are close to the roughness for small indentations. The ratios achieve the value of the standard deviations of $\left(\frac{R_i}{R_0}\right)^{\frac{2}{3}}$ for Sample A indented by Tip 1 and Tip2 at maximum depths of 6 nm and 4 nm, respectively. And the ratios acquire the value of the standard deviation of $\left(\frac{R_i}{R_0}\right)^{\frac{2}{3}}$ for Sample B at 7 nm and 4 nm for Tip 1 and Tip 2, respectively. The slope of the "Tip 2" curve in Fig. 7 is significantly larger than that of the "Tip 1" curve. This indicates that the roughness effect decays faster for a sharper indenter, although it is stronger for such an indenter at very small depths. The slope difference in Fig. 8 is not as significant. Cross-comparing the curves generated by the same indenter on different samples, we find that the roughness effect is stronger and decays faster on the rougher surface. The latter may due to the hardness difference between the two samples. It is concluded that the contact model together with the assumptions and simplifications predicts the variation of indentation hardness measurements well for indentations whose sizes are comparable to the roughness. The roughness effect can be calculated using the procedure presented here before any indentation is made. Note that there is no plastic deformation for the shallowest indentations for the four cases, i.e. the residual depths are zero. For thin film materials, we need to keep the residual depths less than 20% of the film thickness to avoid

the substrate effect on the indentation hardness measurements. The contact model for the roughness effect should still be valid for films thinner than, say 4 nm, since residual depths are already zero for the cases in this study.

6.4 SUMMARY AND CONCLUSIONS

A model for the indentation of surfaces with curvature, such as bumps and asperities is proposed. The power of 2/3 of the R/R_0 is verified experimentally on surface asperities with radii of curvature ranging from 250 nm to 2 μm. The model is then adopted to study the roughness effect on indentation hardness measurements. The concept of the apparent surface properties for a specific indentation is proposed. This gives slightly different surface properties of the same surface for indenters with different tip radii. The ratio of the standard deviation to the mean hardness is compared with the apparent standard deviation of $\left(\frac{R_i}{R_0}\right)^{\frac{2}{3}}$, where R_i is the relative radius of curvature and R_0 is the indenter tip radius. The results show that at very small indentations the ratios of the standard deviations to the mean hardnesses equal the standard deviation of $\left(\frac{R_i}{R_0}\right)^{\frac{2}{3}}$ for all of the sample and indenter combinations. This means that the roughness effect on the indentation hardness measurements can be predicted with only the knowledge of the surface properties and tip radii using the model proposed here.

ACKNOWLEDGEMENTS

This work is supported by the Computer Mechanics Laboratory at the University of California, Berkeley. The samples tested in this report are provided by the IBM Corporation.

Table 1: Mean hardness, standard deviation, and their ratios for random indentation hardness measurements.

Indenter	Hardness Properties	Sample A	Sample B
Tip 1 (186 nm)	Mean (GPa)	16.216	6.213
	Standard Deviation (GPa)	2.661	1.275
	SD/Mean ratio	**0.164**	**0.205**
	Mean (GPa)	17.027	5.948
	Standard Deviation (GPa)	8.718	2.790
	SD/Mean ratio	**0.512**	**0.469**
	Mean (GPa)	16.521	6.545
	Standard Deviation (GPa)	15.348	4.084
	SD/Mean ratio	**0.929**	**0.624**
Tip 2 (56 nm)	Mean (GPa)	16.126	6.180
	Standard Deviation (GPa)	3.527	0.826
	SD/Mean	**0.219**	**0.134**
	Mean (GPa)	16.385	6.951
	Standard Deviation (GPa)	9.962	4.380
	SD/Mean ratio	**0.608**	**0.63**
	Mean (GPa)	14.956	6.025
	Standard Deviation (GPa)	17.484	4.687
	SD/Mean ratio	**1.169**	**0.778**

Table 2: The apparent properties of the surfaces of both samples

Indenter	Apparent surface properties	Sample A	Sample B
Tip 1 (R_0=186 nm)	Mean of radii of curvature (nm)	-32.03	-83.02
	S.D. of radii of curvature (nm)	366.65	2268.93
	S.D. of $(R_i / R_0)^{2/3}$	**0.932**	**0.640**
Tip 2 (R_0=56 nm)	Mean of radii of curvature	-58.45	-98.35
	S.D. of radii of curvature	398.64	2298.80
	S.D. of $(R_i / R_0)^{2/3}$	**1.171**	**0.789**

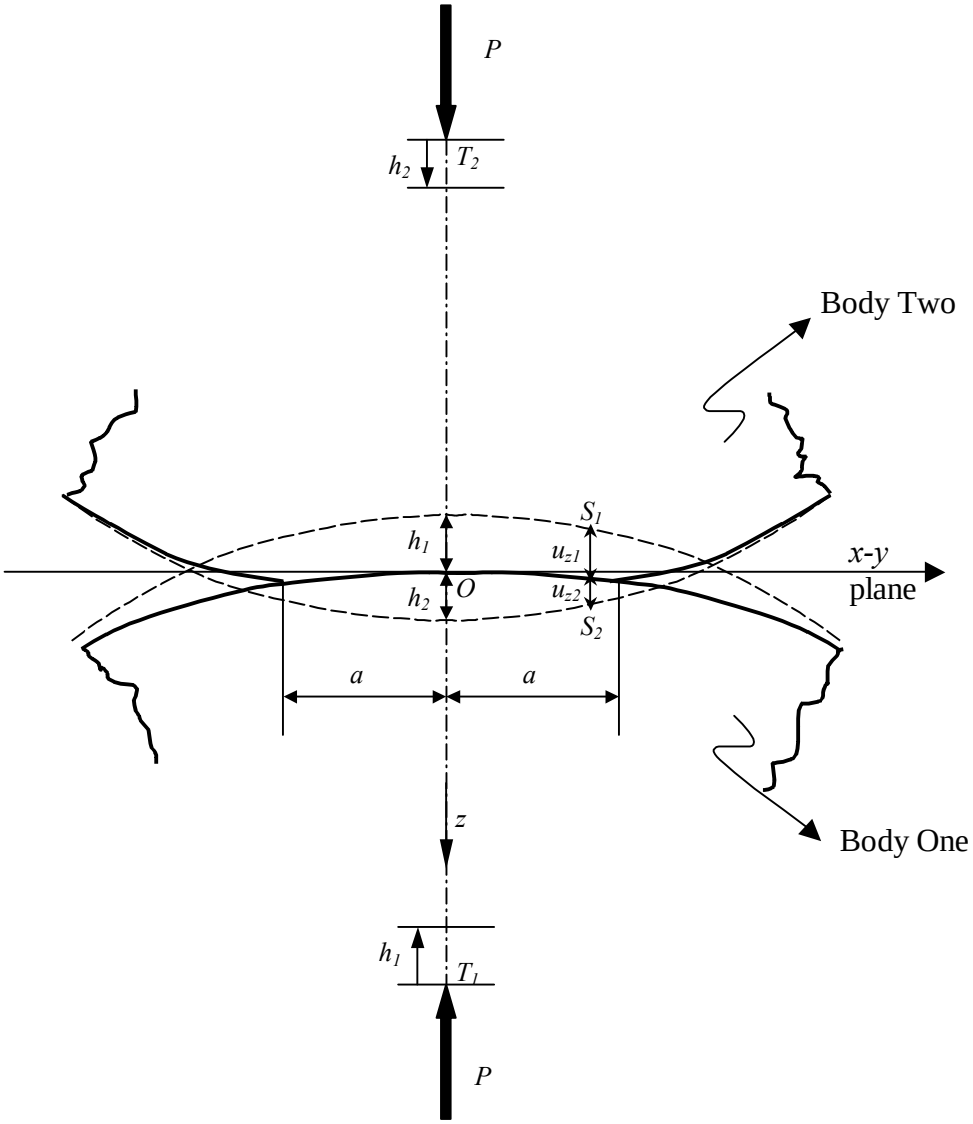

Fig. 1: Contact of two solids of revolution on the areas around their apex points.

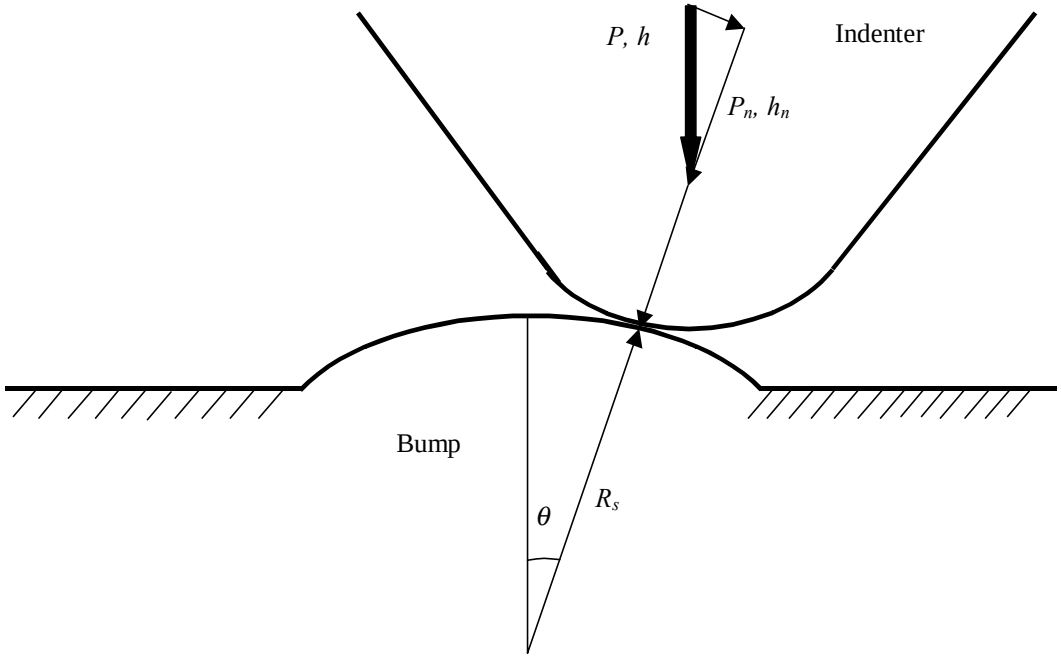

Fig. 2: Indentation on a spherical bump with offsets

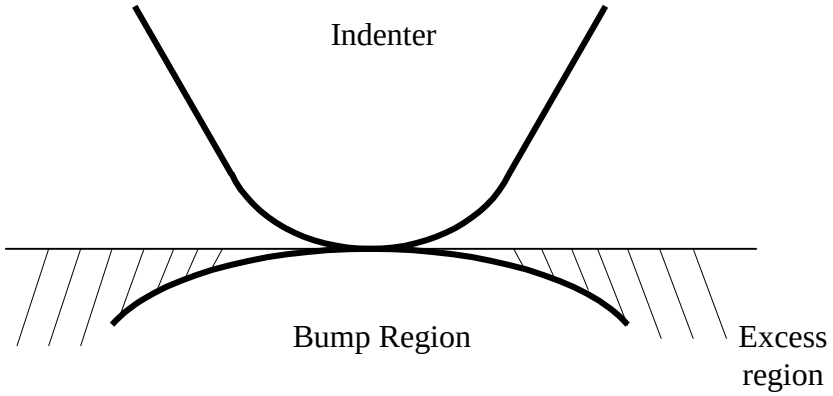

Fig. 3: Illustration of the idea showing that the measured hardness is lower than the true hardness.

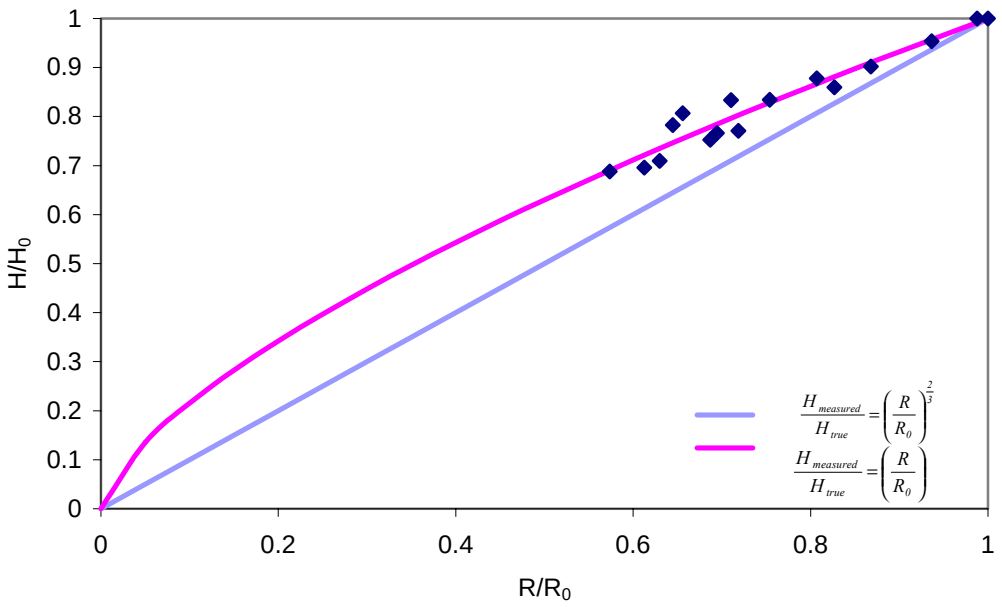

Fig. 4: Indentations on spherical asperities. The data shown agree with the contact model derived from Hertz contact theory.

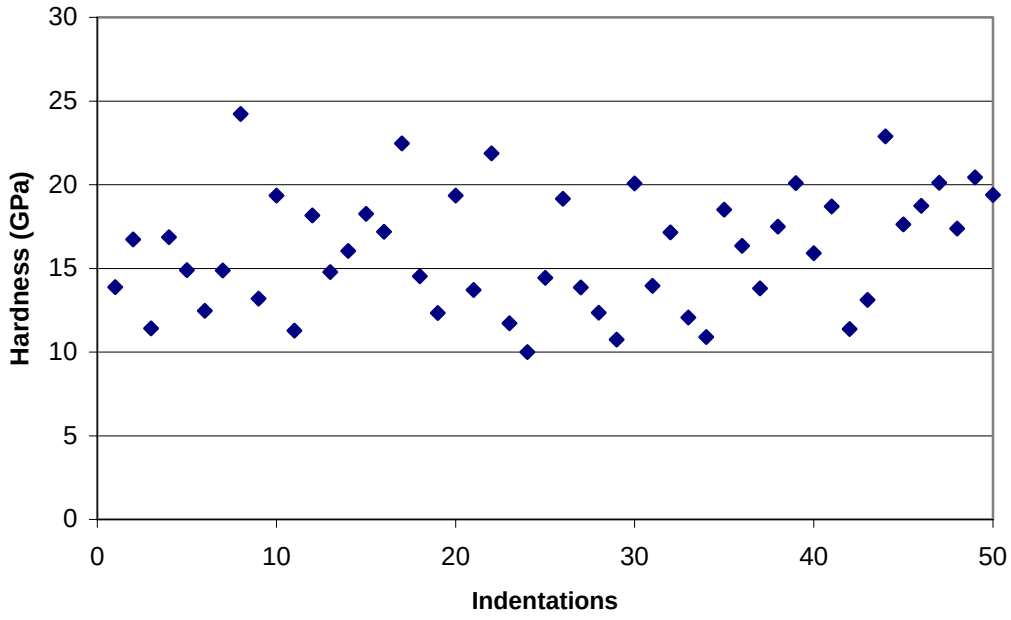

Fig. 5: Random indentations on sample A with the indenter of tip radius of 56 nm.

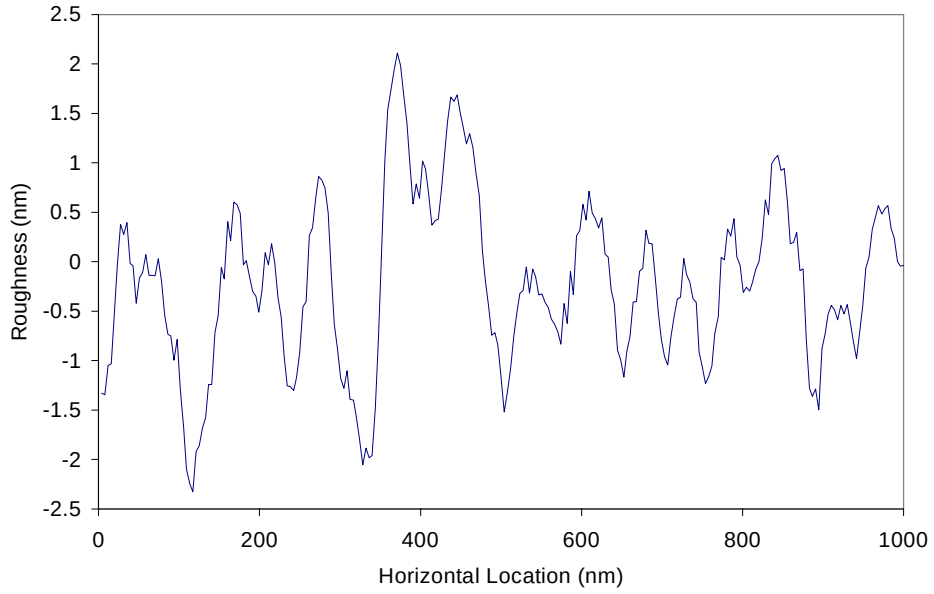

Fig. 6: A typical line of the scanned image of sample A surface. Note that the vertical dimension has been exaggerated.

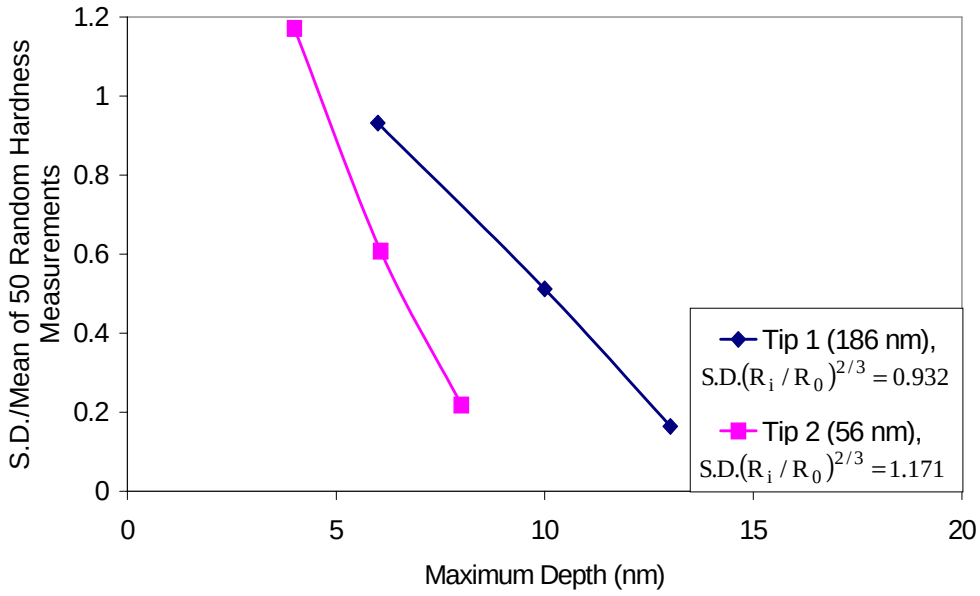

Fig. 7: The ratios of standard deviations to mean hardnesses of Sample A indented by Tip 1 and Tip 2. Each data point represents the result of 50 random indentations. The apparent standard deviations of $(R_i / R_0)^{2/3}$ for both tips are listed in the legend.

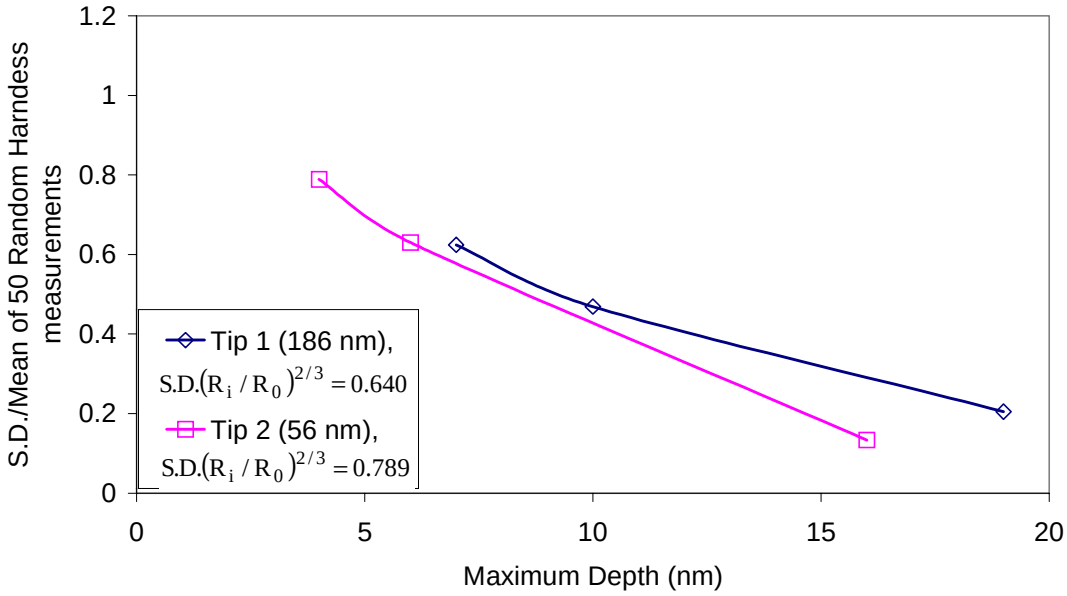

Fig. 8: The ratios of standard deviations to mean hardnesses of Sample B indented by Tip 1 and Tip 2. Each data point represents the result of 50 random indentations. The apparent standard deviations of $(R_i / R_0)^{2/3}$ for both tips are listed in the legend.

REFERENCE

Bobji, M. S., Fahim, M., Biswas, S. K., 1996, "Hardness estimated from the indentation of a spherical body. Some implications for nanoindentation test results", *Tribology Letters*, Vol. 2, pp. 381-391

Greenwood, J. A. and Williamson, J. B. P., 1966, "Contact of nominally flat surfaces", *Proceedings Royal Society*, Vol. A295, pp. 300

Greenwood, J. A., 1967, "The area of contact between rough surfaces and flats", *Transactions of the American Society of Mechanical Engineers*, Vol. 89, pp. 81-91

Johnson, K. L., 1985, "Contact Mechanics", Cambridge University Press, Cambridge, U. K.

Ling, F. F., 1973, "Surface Mechanics", John Wiley & Sons, Inc., New York, pp.173-179

Lo, R. Y., Bogy, D. B., 1997, "On the measurement of nanohardness and elastic modulus of ultra-thin overcoats: effect of W-doping and annealing on the properties of DLC", *Technical Report No.* 97-017, Computer Mechanics Laboratory, Department of Mechanical Engineering, University of California, Berkeley.

Lo, R. Y. and Bogy, D. B., 1999, “Compensating for elastic deformation of the indenter in hardness tests of very hard materials”, *Journal of Materials Research*, Vol. 14, No. 6, pp. 2276-2282

Tabor, D., 1951, “The Hardness of Metals”, Clarendon Press, Oxford